6092 *Chem. Mater.* **2010,** *22,* 6092–6102
DOI:10.1021/cm101587e

CHEMISTRY OF MATERIALS
Article

First-Principles Study of Defective and Nonstoichiometric Sr_2FeMoO_6

Rohan Mishra,[†] Oscar D. Restrepo,[†] Patrick M. Woodward,[‡] and Wolfgang Windl*[,†]

[†]*Department of Materials Science and Engineering, The Ohio State University, Columbus, Ohio 43210, United States, and* [‡]*Department of Chemistry, The Ohio State University, Columbus, Ohio 43210, United States*

Received June 7, 2010. Revised Manuscript Received September 23, 2010

The influence of disorder and stoichiometry-breaking point defects on the structural and magnetic properties of Sr_2FeMoO_6 have been investigated with the help of electronic structure calculations within the spin-polarized GGA+U approach. Defining the chemical potentials of the constituent elements from constitutional defects, we calculate the energetics of the possible point defects in nonstoichiometric Sr_2FeMoO_6 and find transition-metal-ion antisites and oxygen vacancies to be dominant. In nonstoichiometric $Sr_2Fe_{1+x}Mo_{1-x}O_6$ with $-0.75 \le x \le 0.25$, both Fe_{Mo} antisites (for Fe-rich samples or $x > 0$) and Mo_{Fe} antisites (for Mo-rich samples or $x < 0$) lead to a systematic decrease in saturation magnetization. Only Mo_{Fe} antisites destroy the half-metallic character of the electronic structure, since their t_{2g} band crosses the Fermi level for $x \le -0.125$. This leads to a decrease of spin polarization from 100% for $x \ge -0.125$ to 0 at $x \approx -0.75$. Oxygen vacancies also reduce the saturation magnetization, but the half-metallic character and, hence, 100% spin polarization is retained. The optimized unit-cell lattice parameter remains within a relatively narrow range (7.96 Å for $x = +0.25$ to 8.00 Å for $x = -0.75$), despite large changes in composition. In stoichiometric Sr_2FeMoO_6, the saturation magnetization decreases linearly as the Fe/Mo antisite disorder increases, and the half metallicity is lost, because of the t_{2g} states on both Mo_{Fe} and Fe_{Mo}. The spin polarization remains ~100% only for very small amounts of disorder. The calculated disorder formation energies suggest that short-range ordering is favorable in Sr_2FeMoO_6. The calculated results are in excellent quantitative agreement with experimental values, where available.

1. Introduction

Complex oxides with the double perovskite structure ($A_2B'B''O_6$, where A is an alkali, alkaline-earth, or rare-earth metal, B′ and B″ are transition metals) have been studied since the 1960s, to understand the underlying science behind the plethora of interesting electrical and magnetic properties that they display. The discovery of room-temperature colossal magnetoresistance in Sr_2FeMoO_6 in 1998 provided a major impetus for application-driven research.[1] The high Curie temperature of 412 K and high degree of spin polarization make Sr_2FeMoO_6 an ideal candidate for use in "spintronics" devices such as magnetic tunnel junctions and spin injectors. However, defects (antisite disorder and nonstoichiometry) can negatively impact the magnetotransport properties of Sr_2FeMoO_6 and other double perovskites.

The perovskite structure can be described as a network of corner-sharing octahedra with the larger A-site cation filling cuboctahedron (12-coordinate) cavities within this network. In ordered $A_2B'B''O_6$ double perovskites, there is an alternation between $B'O_6$ and $B''O_6$ along all three Cartesian directions. Ideally, the resulting structure is cubic with $Fm\bar{3}m$ space group symmetry. Indeed, above 400 K, Sr_2FeMoO_6 adopts the high-symmetry cubic structure with a cell edge of $a = 7.90$ Å. Below 400 K, the unit cell becomes tetragonal with $I4/m$ space group symmetry and lattice parameters of $a = b = 5.57$ Å and $c = 7.90$ Å, as shown in Figure 1a.[2] The tetragonal distortion is a result of antiphase rotations of the octahedra about the c-axis.[3] However, the effect of the rotations is small and, in the pseudo-cubic supercell (see Figure 1b), leads to differences between a, b, and c on the order of ~0.03 Å. Therefore, to a good approximation, it is possible to use the cubic cell for simulations, which results in enhanced computational speed, because of the additional symmetry.

The electrons associated with the Fe^{3+} ions (with a spin quantum number of $S = {}^5/_2$ arising from the presence of five unpaired electrons with parallel spins) are localized and ferromagnetically coupled with each other. The electrons associated with the Mo^{5+} ions (with $S = {}^1/_2$ arising from the presence of one unpaired electron) are delocalized and aligned antiparallel to the localized Fe^{3+} spins. Since the Fe and Mo atoms are ferrimagnetically coupled with each other, every formula unit has a theoretical

*Author to whom correspondence should be addressed. Tel.: +1-614-247-6900. Fax: +1-614-292-1537. E-mail: windl.1@osu.edu.

(1) Kobayashi, K.-I.; Kimura, T.; Sawada, H.; Terakura, K.; Tokura, Y. *Nature* **1998**, *395*, 677.
(2) Chmaissem, O.; Kruk, R.; Dabrowski, B.; Brown, D. E.; Xiong, X.; Kolesnik, S.; Jorgensen, J. D.; Kimball, C. W. *Phys. Rev. B* **2000**, *62*, 14197.
(3) Woodward, P. M. *Acta Crystallogr., Sect. B: Struct. Sci.* **1997**, *53*, 32.

 Published on Web 10/26/2010

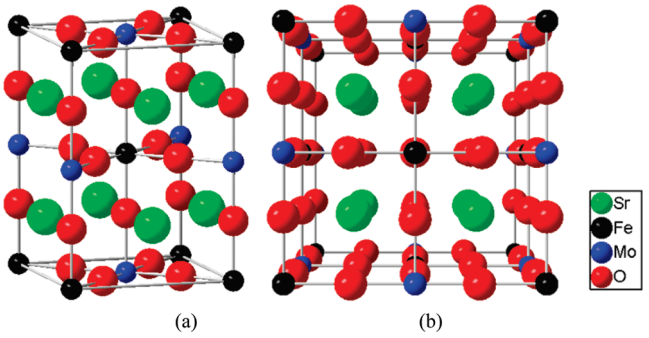

Figure 1. (a) Tetragonal unit cell and (b) 40-atom supercell of Sr_2FeMoO_6.

spontaneous saturation magnetization (M_s) of 4 Bohr magnetons (μ_B). The calculated spin-resolved density of states (DOS) (see Figure 2) shows a finite gap of 1.4−1.5 eV between the valence and conduction bands in the spin-up channel and a metal-like, continuous DOS across the Fermi level (ε_F) in the spin-down channel, as shown previously.[1,4,5] This makes Sr_2FeMoO_6 a half-metal with 100% spin polarization, because only the down-spin bands have a finite density at the Fermi level. The experimentally observed Curie temperature (T_C) is 412 K.[1,2,4]

The synthesis of "perfect" Sr_2FeMoO_6 is exceedingly difficult. Hence, most, if not all, samples have a non-negligible concentration of defects. Control of the stoichiometry and defects becomes even more challenging upon moving from bulk samples to thin films. Possible defects include nonstoichiometry due to excess Mo or Fe, antisite disorder due to the simultaneous formation of Fe_{Mo} and Mo_{Fe}, oxygen vacancies (V_O), and the formation of extended phases. Some of these defects have been shown to affect the electronic and magnetic properties in a substantial way. Experiments show that the M_s and T_C values change systematically with the composition x in $Sr_2Fe_{1+x}Mo_{1-x}O_6$;[6] the magnetization changes with the V_O concentration,[7] and the M_s values and spin polarization vary with the order parameter ξ:[8,9]

$$\xi = 1 - \frac{\text{the number of antisites in sublattice}}{\text{lattice sites in sublattice}}$$

Some level of antisite disorder is currently thought to be inevitable, even in stoichiometric bulk samples.

The apparent inevitability of defects makes it imperative to understand how various defects affect the magnetic and magnetotransport properties of Sr_2FeMoO_6. Thus, we have been studying the influence of the different types of point defects on the properties of Sr_2FeMoO_6, using state-of-the-art density functional theory (DFT) calculations.

We also compare our results to the limited number of previous publications that have addressed some of the questions studied in the present paper and discuss the differences in the results. We also predict, for the first time, the thermodynamic stability of the competing point defects by calculating their formation energies. For this, we suggest deriving the needed chemical potentials of the different elements from ab initio calculations, using the concept of constitutional defects.[10]

2. Method

2.1. Computational Framework. The present study was performed with the Vienna ab initio simulation package (VASP),[11] using projector augmented wave (PAW) pseudopotentials[12] and a spin-polarized generalized gradient approximation[13] (GGA) to DFT. A plane-wave cutoff energy of 500 eV was used throughout. Monkhorst-Pack k-point meshes[14] were used to sample the Brillouin zone, where the mesh division N_i for the lattice vectors a_i was chosen such that $N_i a_i$ was as close as possible to 32 Å for structural relaxations and 80 Å for electronic calculations.

Transition-metal (TM) oxides have localized electrons in their d-orbitals. In strongly correlated TM compounds, the localized d-electrons have energies near the Fermi energy (ε_F). Normal DFT calculations often do not describe the electronic and magnetic properties of such systems correctly. Many previous DFT studies have shown that neglecting to correct for the strong correlation in Sr_2FeMoO_6 often leads to discrepancies between calculated and experimentally observed properties.[4,5,15] Therefore, we have explicitly included this strong correlation effect in our calculations, using the so-called GGA+U approach, which has been shown to significantly improve predictions of thermodynamic, electronic, and magnetic properties of TM oxides.[16−18] The applied corrections have been found to be crucially important for the localized electrons on Fe. The case of Mo atoms is different, where it is believed that the 4d electrons move between the hybridized orbitals of Fe and Mo and, thus, are not localized, but rather itinerant.[4] For our calculations, the rotationally invariant Dudarev approach[19] to GGA+U has been employed. For Fe, values of U = 3.0 eV and J = 0.95 eV was used as suggested in recent literature, resulting in U_{eff} = 2.05 eV.[17] In addition, we have also tested adding a value of U_{eff} = 2.85 eV for the p-orbital electrons in O, to probe the effect of any strong localization that

(4) Sarma, D. D.; Mahadevan, P.; Saha-Dasgupta, T.; Ray, S.; Kumar, A. *Phys. Rev. Lett.* **2000**, *85*, 2549.
(5) Saha-Dasgupta, T.; Sarma, D. D. *Phys. Rev. B* **2001**, *64*, 64408.
(6) Topwal, D.; Sarma, D. D.; Kato, H.; Tokura, Y.; Avignon, M. *Phys. Rev. B* **2006**, *73*, 94419.
(7) Töpfer, J.; Kircheisen, R.; Barth, S. *J. Appl. Phys* **2009**, *105*, 07D712.
(8) Huang, Y. H.; Karppinen, M.; Yamauchi, H.; Goodenough, J. B. *Phys. Rev. B* **2006**, *73*, 104408.
(9) Panguluri, R. P.; Xu, S.; Moritomo, Y.; Solovyev, I. V.; Nadgorny, B. *Appl. Phys. Lett.* **2009**, *94*, 12501.
(10) Hagen, M.; Finnis, M. W. *Philos. Mag. A* **1998**, *77*, 447.
(11) Kresse, G.; Hafner, J. Phys. Rev. B **1993**, *47*, 558 (R);**1994**, *49*, 14251.
(12) Blöchl, P. E. *Phys. Rev. B* **1994**, *50*, 17953.
(13) Wang, Y.; Perdew, J. P. *Phys. Rev. B* **1991**, *44*, 13298.
(14) Monkhorst, H. J.; Pack, J. D. *Phys. Rev. B* **1976**, *13*, 5188.
(15) Stoeffler, D.; Colis, S. *Mater. Sci. Eng. B* **2006**, *126*, 133.
(16) Anisimov, V. I.; Zaanen, J.; Andersen, O. K. *Phys. Rev. B* **1991**, *44*, 943.
(17) Zhu, X. F.; Li, Q. F.; Chen, L. F. *J. Phys.: Condens. Matter* **2008**, *20*, 75218.
(18) Fang, Z.; Terakura, K.; Kanamori, J. Phys. Rev. B **2001**, *63*, 180407(R).
(19) Dudarev, S. L.; Botton, G. A.; Savrasov, S. Y.; Humphreys, C. J.; Sutton, A. P. *Phys. Rev. B* **1998**, *57*, 1505.

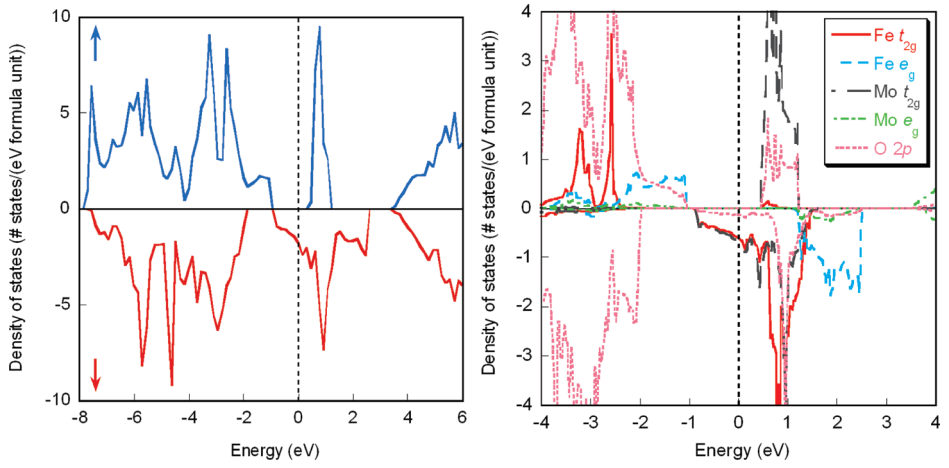

Figure 2. (a) Total density of states (DOS) for ordered Sr_2FeMoO_6 and (b) atom and orbital resolved DOS showing the Fe, Mo, and O states present near the Fermi level.

may be present as a result of hybridization with the Mo 4d and Fe 3d orbitals, and adding a value of $U_{eff} = 1$ eV for Mo, to examine if the Mo electrons are indeed itinerant.

To test if the use of a cubic cell instead of the tetragonal minimum-energy geometry is justified, we calculated lattice parameters, total energies, and magnetization for 40-atom supercells with $x = -0.75$, -0.5, -0.25, 0, and 0.25. The asymmetry in the lattice constants a and c was found to be well below 0.1% for all compositions, with the exception of $x = -0.5$, with a still small value of 0.68% (0.05 Å), corresponding to cell volume differences between -0.19% and $+0.05\%$. Changes in the total energy between cubic and tetragonal phases were also small, between 10 meV and 80 meV for the 40-atom cell, with increasing difference with decreasing x. All changes in saturation magnetization were found to be $< 3\%$. Since changes of this magnitude do not affect any of our findings and conclusions in the following, we restricted all further calculations to cubic supercells, which decreases the computational effort considerably and allows our calculations to be extended to systems with up to 160 atoms.

To probe the effects of cell size, we studied defects in supercells of different size: a tetragonal unit cell containing 20 atoms (or 2 f.u. (where f.u. denotes formula units)) of Sr_2FeMoO_6, as shown in Figure 1a; a supercell of 40 atoms (or 4 f.u.), as shown in Figure 1b, and a $2 \times 2 \times 2$ supercell of the face-centered cubic (fcc) primitive cell containing 80 atoms (or 8 f.u.). In addition, a single calculation using a supercell containing 160 atoms (or 16 f.u.) was performed to probe the effects of a very small amount of disorder ($\xi = 93.75\%$) on M_s and spin polarization. The calculations were constrained to cubic symmetry, to make the computational effort more manageable. Atomic positions and lattice constants were optimized for all calculations at zero external pressure.

Although the spin-resolved density of states (DOS), the atom- and orbital-resolved DOS, lattice parameters, and magnetization are direct outputs of a VASP calculation, we obtain the spin polarization of a structure, which we define as

$$P = \frac{n_\downarrow - n_\uparrow}{n_\downarrow + n_\uparrow} \tag{1}$$

from postprocessing of the DOS, where $n_\uparrow$ and $n_\downarrow$ are the numbers of conduction electrons with spin up and down, respectively. For simple systems at very low temperatures with few band crossings in the immediate vicinity of the Fermi energy ε_F, the number of spin-up or spin-down electrons is proportional to the respective spin-resolved DOS at the ε_F level and can be replaced by the corresponding DOS values in eq 1.[20] For a more complex system with band crossings and larger numbers of bands in the vicinity of the ε_F level (such as the defective systems studied in the present paper), the DOS may change very rapidly over small energy intervals (either as a real effect or as an artifact of the DOS calculation method). In this case, we found that calculating the actual number of conduction electrons, using the relation

$$n_{\downarrow,\uparrow} = \int_{\varepsilon_F}^{\infty} g_{\downarrow,\uparrow}(E) f(E)\, dE \tag{2}$$

to converge better and give more-sensible results, where $g_{\uparrow,\downarrow}$ is the spin-polarized DOS and f is the Fermi function,

$$f(E) = [\exp(\frac{E - \varepsilon_F}{k_B T}) + 1]^{-1}$$

centered at the ε_F. The calculations in the following have been carried out for a temperature of 300 K. This approach gives the same results as direct replacement of the number of electrons by DOS values for cases with smooth and flat DOS curves at the Fermi level, but significantly decreases scattering of the polarization values otherwise.

2.2. Defect Energetics. Since point defects break the stoichiometry, chemical potentials (μ) of the constitutive

(20) Mazin, I. I. *Phys. Rev. Lett.* **1999**, *83*, 1427.

elements must be calculated to compare the thermodynamic stability of different defects. Assessing μ for each of the elements in a multicomponent system is challenging. In our case, the total energy of 1 f.u. of perfect Sr_2FeMoO_6 can be expressed as

$$2\mu_{Sr} + \mu_{Fe} + \mu_{Mo} + 6\mu_O = \frac{E(N, \mathrm{SFMO})}{N} \quad (3)$$

where the subscript denotes the chemical elements, N is the number of f.u. in the supercell, and $E(N, \mathrm{SFMO})$ is the calculated total energy of the supercell. The formation energy (E_f) of any point defect such as V_O can be calculated with the help of the chemical potentials. For the example of V_O,

$$E_f(V_O) = E(N, V_O) - E(N, \mathrm{SFMO}) + \mu_O \quad (4)$$

where $E(N,V_O)$ is the energy of an N f.u. supercell of Sr_2FeMoO_6 with a single V_O. Similarly, the E_f value of an antisite, such as an Fe_{Mo} antisite, can be expressed as

$$E_f(\mathrm{Fe_{Mo}}) = E(N, \mathrm{Fe_{Mo}}) - E(N, \mathrm{SFMO}) - \mu_{Fe} + \mu_{Mo} \quad (5)$$

In previous works, the chemical potential of a particular element has been approximated by the energy of a single atom of that element under vacuum, which can lead to misleading results, as discussed by Hagen and Finnis,[10] who have suggested a method for calculating each μ in a binary system using the concept of constitutional defects. The basic assumption is that all nonstoichiometries are accommodated by point defects and, more specifically, by that combination of point defects with the lowest total energy cost, which are then the constitutional defects. Sen and Windl have extended this approach to ternary perovskites.[21] Building upon that, we have formulated a generalized model applicable to any N-component system, which is summarized in the following and discussed in detail elsewhere.[22] As a note, this approach starts from the assumption of small levels of nonstoichiometry to define the chemical potentials.

For an N component system, we need N μ values and, hence, N equations to calculate them. We assume $(N-1)$ "constitutional" defects to be present in the system. A defect is constitutional if it has a lower formation energy than all other defects or defect combinations yielding the same (non)stoichiometry. Since this is the ground state for the considered stoichiometry, the formation energy of a constitutional defect must be zero, which, in certain cases, such as V_O (eq 4) allows for immediate calculation of the chemical potential of oxygen. By combining the expressions for the postulated constitutional defects (eqs 4 and 5 and similar equations) with eq 3, we get N equations which can be solved to calculate all the μ values. We can then determine the E_f values of all the other defects in the system. Our approach consists of taking all possible combinations of $(N-1)$ constitutional defects that can form in the system, calculating the chemical potentials for them (using eqs 3−5 and the requirement that $E_f = 0$ for constitutional defects), and determining the E_f value of the remaining defects. Only those combinations for which the E_f values of all the remaining defects are greater than zero are sensible (if a defect has $E_f < 0$, it would be a constitutional defect, contradicting the initial assumption). This approach gives results in agreement with the previous procedures by Hagen and Finnis[10] and Sen and Windl,[21] but it does not restrict the number of elements in the compound.

(21) Sen, D.; Windl, W. *J. Comput. Theor. Nanosci.* **2007**, *4*, 1.
(22) Mishra, R.; Restrepo, O. D.; Windl, W. Unpublished work.

3. Results and Discussion

3.1. Defect-Free Sr_2FeMoO_6. The calculated (symmetry restricted) lattice parameters of $a = b = c = 7.97$ Å are roughly 1% larger than the experimental values of $a = b = \sqrt{2} \times 5.57$ Å $= 7.88$ Å and $c = 7.90$ Å.[1,2] Figure 2a shows the spin-resolved density of states (DOS) for the 40-atom supercell. As shown in Figure 2b, the spin-up band below ε_F has contributions from Fe t_{2g} and e_g states and O 2p states, while the conduction band (immediately above ε_F) is dominated by Mo t_{2g} states. The spin-down band is continuous through the Fermi energy with Mo t_{2g}, Fe t_{2g}, and O 2p contributions. Near-equal contributions of the Mo t_{2g} and Fe t_{2g} orbitals are consistent with a fully delocalized picture of the spin-down electrons. Since there are only spin-down states in the immediate vicinity of the Fermi level, we find a spin polarization of 100%. We calculate M_s, which is the sum of the local magnetic moments of the individual ions, to be 4.0 μ_B/f.u. The Fe spins are all ferromagnetically coupled with a magnetic moment of 3.9 μ_B/atom, while the Mo spins couple antiparallel to the Fe atoms (ferrimagnetic coupling) with a magnetic moment of −0.4 μ_B/atom. We also find that the O atoms have a small magnetic moment between 0.06 μ_B/atom and 0.09 μ_B/atom, aligned parallel to the moments of the Fe atoms. Adding all the moments, we get $M_s = 4.0$ μ_B/f.u., which is consistent with previous studies.[1,4,5,17]

3.2. Constitutional Defects in $Sr_2Fe_{1+x}Mo_{1-x}O_6$. Oxygen vacancies are a common defect in a diverse group of perovskite oxides, and they have been observed in Sr_2FeMoO_6.[7] Hence, for Sr_2FeMoO_6, we only need to consider two additional constitutional defects. Calculating the defect energies in Sr_2FeMoO_6 using the approach outlined in section 2.2, we find that to accommodate the nonstoichiometry in Fe and Mo (i.e. $Sr_2Fe_{1+x}Mo_{1-x}O_6$), antisites are more favorable than vacancies. More specifically, for Mo-rich material, the excess Mo should, to the greatest part, be accommodated by the constitutional Mo_{Fe} antisites, while Fe_{Mo} antisites have an energy penalty of 1.6 eV. V_{Fe} and V_{Mo} have formation energies of 2.7 and 5.2 eV, respectively, in comparison to Mo_{Fe} ($E_f(Mo_{Fe}) = 0$ by definition). For Fe-rich material, the situation is opposite, with Fe_{Mo} as the constitutional defect and Mo_{Fe} being ~1.5 eV higher in formation energy. In this case, V_{Fe} and V_{Mo} have formation energies of 6.9 and 7.9 eV, respectively. The formation energies of the

Table 1. Formation Energy (E_f) of the Different Point Defects for Mo-Rich and Fe-Rich Sr_2FeMoO_6

	Formation Energy (eV)[a]	
point defect	Mo-rich	Fe-rich
V_O	0	0
V_{Fe}	2.7	6.9
V_{Mo}	5.2	7.9
V_{Sr}	5.6	2.2
Mo_{Fe}	0	1.5
Fe_{Mo}	1.5	0
Fe_{Sr}	7.7	0
Sr_{Fe}	0	7.7
Mo_{Sr}	10.6	4.4
Sr_{Mo}	1.4	7.6

[a] The defects with $E_f = 0$ are constitutional defects.

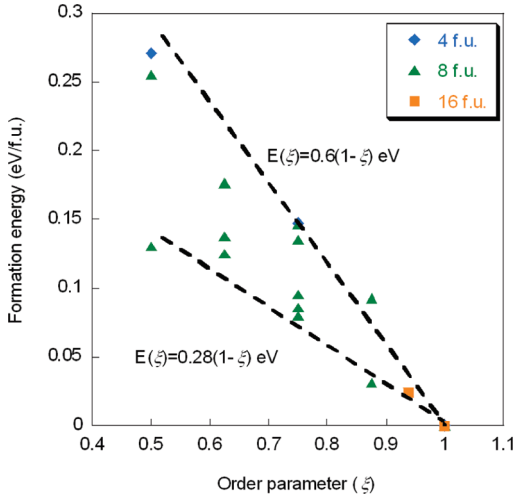

Figure 3. Energy of a formula unit of disordered Sr_2FeMoO_6 as a function of the order parameter ξ. For a given value of ξ, structures can have different energies, depending on the arrangement of the antisites.

different point defects for both Mo-rich and Fe-rich Sr_2FeMoO_6, based on our approach of constitutional defects, are shown in Table 1.

3.3. Energetics of Antisite Disorder in Stoichiometric Sr_2FeMoO_6. For stoichiometric Sr_2FeMoO_6 with disorder in the Fe/Mo sublattice in the form of antisite pairs, we find a range of energies for any given amount of disorder, as shown in Figure 3. The slopes of the lower and upper boundaries give the cost of creating a single pair of antisites to be between 0.28 eV and 0.6 eV, with the exact value being dependent not only on the amount of disorder, but also on their specific arrangement. Similarly, the orientation of the magnetic moment on the Mo_{Fe} antisite atoms is found to be strongly dependent on the amount of Fe/Mo neighbors. A careful analysis of the local environment around the antisites suggests that the energy is strongly dependent on the nearest neighbors. More interestingly, we find that antisite pairs placed next to each other have a lower formation energy than antisite pairs that are placed far apart. As an example, the formation energy for one pair of nearest-neighbor Fe/Mo antisites in an 8 f.u. supercell (i.e., $\xi = 0.875$) is 0.5 eV lower than the formation energy for a third-nearest-neighbor arrangement (considering only the Fe/Mo sublattice). This suggests the presence of short-range order, even in a disordered Sr_2FeMoO_6 sample, as observed recently by Meneghini et al.[23] The change in properties due to the antisite constitutional defects are in excellent agreement with experiments, as discussed below, giving a posteriori support to the energy calculations.

Table 2. Formation Energy (E_f) of Unrelaxed and Relaxed Supercells with Varying Amounts of Disorder, along with the Number of Type I and Type II Bonds in Each Disordered Supercell

	E_f (eV) (First Principles)		Number of Bonds		
ξ	unrelaxed	relaxed	Type I	Type II	E_f (eV) (model)[a]
0.125	2.19	0.74	12	0	2.16
0.125	1.98	0.25	10	1	1.91
0.25	4.16	1.17	24	0	4.31
0.25	4.07	0.64	20	2	3.82
0.25	3.73	1.07	20	2	3.82
0.375	5.30	1.39	26	5	5.24
0.375	4.67	1	22	7	4.75

[a] The modeled E_f value is a summation over the Type I and Type II bond energies, with values of 0.18 and 0.11 eV, respectively.

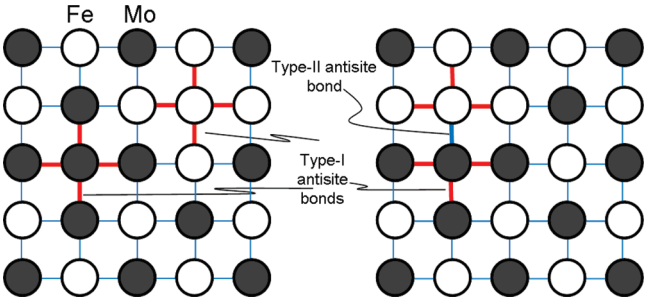

Figure 4. Two-dimensional slice showing separated (left) and neighboring (right) pairs of antisite defects $Fe_{Mo} + Mo_{Fe}$. The thicker red lines show the Type I Fe−O−Fe and Mo−O−Mo antisite bonds, and the thick blue line represents the Type II antisite bond.

To probe the underlying reasons behind this attraction of antisites, we compare the energies of 8 f.u. supercells of Sr_2FeMoO_6 with different arrangements of antisites for $\xi = (0.875, 0.75, \text{and } 0.625)$, before and after relaxation from the perfect Sr_2FeMoO_6 supercell, as shown in Table 2. We begin with an analysis of the unrelaxed structures. Rock-salt ordering of the Fe and Mo atoms in perfect Sr_2FeMoO_6 leads to the formation of Fe−O−Mo bonds, with each Fe atom surrounded by 6 Mo atoms and vice versa. Antisite disorder breaks this pattern, resulting in the formation of Fe_{Mo}−O−Fe and Mo_{Fe}−O−Mo bonds, the exact number of which is based on the separation between the Mo_{Fe} and Fe_{Mo} antisites. As an example, we consider an 8 f.u. supercell with just one pair of antisites ($\xi = 0.875$). Separated antisites form six Fe_{Mo}−O−Fe and six Mo_{Fe}−O−Mo bonds, whereas neighboring antisites form five Fe_{Mo}−O−Fe bonds, five Mo_{Fe}−O−Mo bonds, and one Fe_{Mo}−O−Mo_{Fe} bond. A two-dimensional depiction of these two cases is shown in Figure 4.

Table 2 shows that less energy is needed to form neighboring antisites than that needed to form separated antisites (1.98 eV vs 2.19 eV in the unrelaxed case). If we assume that the energy penalty is entirely due to the

(23) Meneghini, C.; Ray, S.; Liscio, F.; Bardelli, F.; Mobilio, S.; Sarma, D. D. *Phys. Rev. Lett.* **2009**, *103*, 046403.

formation of Fe_{Mo}−O−Fe and Mo_{Fe}−O−Mo bonds, we can estimate the energy penalty in terms of a local bond picture. Because there is no way to separate the Fe_{Mo}−O−Fe contribution from the Mo_{Fe}−O−Mo contribution, we label these as Type I antisite bonds and assume that they are higher in energy than Fe−O−Mo bonds by equal amounts. For the case of separated antisites, there are 12 Type I antisite bonds, and we can estimate the energy penalty per bond to be 2.19 eV/12 = 0.182 eV. If we now assume that this energy penalty is transferrable, the system with neighboring antisites should be higher in energy by 10×0.182 eV = 1.82 eV, which accounts for 92% of the total calculated energy of 1.98 eV. The remaining energy penalty is likely associated with the formation of the Fe_{Mo}−O−Mo_{Fe} bond that connects neighboring antisites. We will refer to Fe_{Mo}−O−Mo_{Fe} bonds as Type II antisite bonds. Using a least-squares fit for all of the remaining unrelaxed supercells, we determine the energy of the Type II antisite bonds to be 0.11 eV. Table 2 shows our results for a range of disordered supercells. The fact that the energies can be fitted well by this (local) bond energy model indicates unequivocally that Coulombic interactions between the antisites are negligible, as expected for a metallic conductor. Thus, the lower energy for Type II bonds, compared to Type I bonds, partially explains the attraction between antisites and the experimentally observed short-range ordering.[23]

Next, we consider the effect of relaxation. As shown in Table 2, we find that the formation energy decreases strongly with relaxation, by values that range from 66% to 87% of the unrelaxed values. Therefore, changes in the metal−oxygen bond lengths in the vicinity of the antisite defects play an important role in stabilizing the formation of such defects.

Examining the strain contribution in more detail, we find that relaxation effects are strongest for nearest-neighbor antisites. For the example of the 8 f.u.-cell calculations for $\xi = 0.875$, we find the Fe_{Mo}−O and Mo_{Fe}−O bond lengths along the connection line between the antisites change, from 2.026 Å and 1.958 Å in perfect Sr_2FeMoO_6 to 2.012 Å and 1.979 Å, respectively, for separated antisites. In contrast, the respective bond lengths in the case of neighboring antisites are 2.231 Å and 1.912 Å. Thus, these Fe_{Mo} and Mo_{Fe} atoms, in the latter case, have a separation that is 4% (0.16 Å) larger than the perfect Sr_2FeMoO_6 Fe−O−Mo distance of 3.984 Å. We also find that this relaxation is very local and anisotropic. It is accommodated by a shortening of the Fe_{Mo}−O bond lying along the connection line between the antisites and pointing away from the Mo_{Fe} atom by −3.9% (0.08 Å) and a similar elongation of the corresponding Mo_{Fe}−O bond by 2.3% (0.04 Å), such that the sum of the four bonds discussed (O−Mo_{Fe}−O−Fe_{Mo}−O) differs by only +1.4% (0.12 Å) from that in perfect Sr_2FeMoO_6. Interestingly, the lengths of the bonds to O atoms perpendicular to the connection line between the antisites remain identical to those in the case of widely separated antisites.

We also perform a Bader analysis[24] to determine changes in the charge values of the different ions. In a Bader analysis,[25] the zero flux surface, on which the electron density is minimal, is determined for each atom and encloses its Bader volume. The number of electrons on each atom is determined by integrating the charge density within the Bader volume, which is then subtracted from the initial number of electrons to get the Bader charge.[26] We find that the observed elongation of the Fe_{Mo}−O−Mo_{Fe} bond is correlated with a change in the Bader charges associated with the Fe_{Mo} and Mo_{Fe} atoms. Although in perfect Sr_2FeMoO_6, the Bader charge associated with a Fe atom is $-1.30e$, the same for the Fe_{Mo} atom for the nearest-neighbor antisite pair is $-1.25e$, thus indicating that the Fe_{Mo} atom goes to a lower oxidation state, when neighboring the Mo_{Fe} antisite, which may occur to alleviate strain. Similarly, the Bader charge on this Mo_{Fe} atom changes from $-1.62e$ in perfect Sr_2FeMoO_6 to $-1.65e$, indicating a shift to a higher oxidation state. In contrast, the change in Bader charges on well-separated Fe_{Mo} and Mo_{Fe} antisites is much smaller (charges of $-1.29e$ and $-1.63e$, respectively).

3.4. Nonstoichiometric Sr_2FeMoO_6. Sr_2FeMoO_6 can be Mo-rich through the creation of either Fe-vacancies (V_{Fe}) or Mo_{Fe} antisites and vice versa for the Fe-rich case. Our calculations of the formation energies of the point defects (see section 3.2) have shown that antisites are energetically more favorable than vacancies and are the constitutional defects that accommodate nonstoichiometry. Thus, only the effect of antisites is discussed in this section.

3.4.1. $Sr_2Fe_{1+x}Mo_{1-x}O_6$: $x > 0$ (Fe-Rich). For this case, we created Fe_{Mo} antisite defects to achieve different nonstoichiometries and calculated the corresponding change in structural and magnetic properties. We observe that both the lattice parameter and the M_s values decrease as x increases, as shown in the Fe-rich part of Figure 5a, which is similar to previously reported theoretical results.[17] However, the half-metallicity is retained (only spin-down electrons are in the immediate vicinity of the Fermi level), resulting in full spin polarization (the Fe-rich part of Figure 6). The decrease in M_s is essentially due to the ferrimagnetic spin of the Fe atoms on the Mo sites. This is similar to the Monte Carlo results reported by Ogale et al.[27] Ferrimagnetic coupling contradicts the model suggested by Saha-Dasgupta et al.[5] This discrepancy is likely due to the fact that the earlier work did not use the DFT + U approach to correct for strong on-site correlations. Our calculations suggest that the ferrimagnetically coupled Fe_{Mo} supercell has a lower energy than that of the ferromagnetically coupled Fe_{Mo} supercell, by ∼0.68 eV/antisite.

(24) Bader, R. F. W. *Atoms in Molecules: A Quantum Theory*; Oxford University Press: New York, 1990.

(25) Henkelman, G.; Arnaldsson, A.; Jónsson, H. *Comput. Mater. Sci.* **2006**, *36*, 254.

(26) Henkelman, G. Bader Charge Analysis. Available via the Internet at http://theory.cm.utexas.edu/vtsttools/bader/, accessed Sept. 21, 2010.

(27) Ogale, A. S.; Ramesh, R.; Venkatesan, T. *Appl. Phys. Lett.* **1999**, *75*, 537.

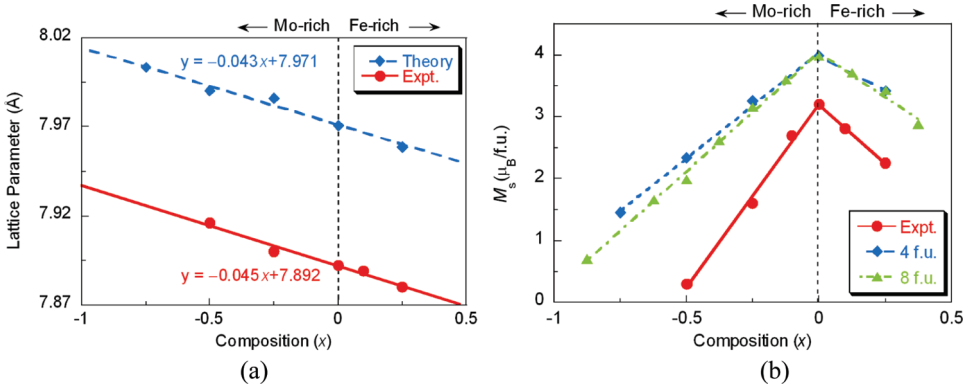

Figure 5. Variation of (a) lattice parameter and (b) M_s for $Sr_2Fe_{1+x}Mo_{1-x}O_6$ compositions with different values of x. Experimental values are taken from ref 6.

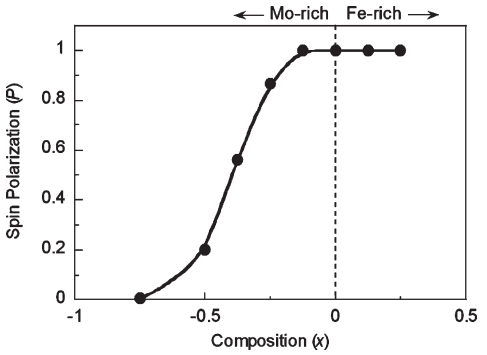

Figure 6. Spin polarization in $Sr_2Fe_{1+x}Mo_{1-x}O_6$, as a function of the composition x. The line is the fit of an error function to the calculated values (dots), and the fitted line is present to guide the eye.

The latter case also leads to an increased M_s value of 4.9 μB/f.u., which is in direct contradiction to the experimentally observed decrease in M_s,[6] thus supporting our result of ferrimagnetic coupling.

In a separate GGA+U study, Stoeffler et al.[28] reported the ferromagnetic coupling between the Fe_{Mo} antisites and Fe_{Fe} atoms to be energetically lower than their ferrimagnetic coupling, by 0.078 eV/antisite. However, they used a 20-atom supercell and changed the lattice parameters while keeping the internal coordinates of the atoms fixed. Our results suggest that, for the smaller 20-atom supercell with a higher concentration of antisites (50%), the ferrimagnetic phase is energetically lower than the ferromagnetic phase, by only 0.01 eV/antisite, after complete structural relaxation. This shows that computational modeling of the favored alignment, ferromagnetic versus ferrimagnetic, of Fe_{Mo} antisite defects is highly sensitive to the size of the supercell for cases where the latter is too small, and to the degree of structural relaxation.

3.4.2. $Sr_2Fe_{1+x}Mo_{1-x}O_6$: $x < 0$ (Mo-Rich). For the Mo-rich case, we created cells of different stoichiometries with Mo_{Fe} antisites. As the samples became increasingly Mo-rich, the lattice parameter increased steadily while the M_s value decreased linearly, as shown in the Mo-rich part of Figure 5a. Upon increasing the Mo nonstoichiometry, additional bands with Mo t_{2g} character, coming predominantly from the Mo_{Fe} atoms (with a small share from Mo_{Mo} atoms), were observed in the majority channel valence band just below the Fermi level. Figure 7a shows the total DOS for $x = -0.125$. Upon increasing the Mo nonstoichiometry further, these additional bands were observed to cross the Fermi level and destroy the half-metallic character of the compound, as shown in Figure 7b, which plots the total DOS for $x = -0.25$. Therefore, we conclude that $Sr_2Fe_{1+x}Mo_{1-x}O_6$ undergoes a half-metal-to-metal transition in the range of $-0.125 \geq x \geq -0.25$. This transition, with a gradual increase in Mo nonstoichiometry, is also manifested in the evolution of spin polarization as a function of composition (the Mo-rich part of Figure 6), which follows an approximately sigmoidal curve, until $x \approx -0.75$, where the spin polarization is completely destroyed. Hence, our calculations indicate that full spin polarization extends into the Mo-rich region up to $x \approx -0.125$, which suggests that one should be able to grow fully spin-polarized material, even if growth parameters may cause the composition to deviate slightly from the stoichiometric case.

The size of the supercell (and, therefore, the degree of translational symmetry) has a very strong effect on the results, when going from a 20-atom cell to a 40-atom cell. For a 20-atom supercell with $x = -0.5$, the M_s value is 20% larger than that for a 40-atom supercell. However, the difference between 40- and 80-atom supercells is small, as shown in Figure 5b.

The slope of the change in lattice parameter with composition due to antisite defects, shown in Figure 5a (-0.043 Å/x) is in good agreement (within 4%) with the experimental slope of -0.045 Å/x,[6] supporting our finding of antisites as the constitutional defects. Our values are also similar to previous theoretical results.[17] In contrast, stoichiometry changes controlled by vacancies would contradict the experimental trends.[29] Although the slope of the lattice constant versus x for antisites is the same on both sides (-0.04 Å/x), it would be zero for the Mo-rich case and -0.23 Å/x for the Fe-rich case, with

(28) Stoeffler, D.; Etz, C. *J. Phys.: Condens. Matter* **2006**, *18*, 11291.

(29) Since the $Fe_{1+x}Mo_{1-x}$ concentration dependence that describes the stoichiometry for antisite-dominated systems does not work for V-dominated systems (where Fe-rich material should be described by $FeMo_{1-x}$), we consider for this comparison the linearized ratio of Fe over Mo concentration, which corresponds to $(1 + 2x)$ for the case of antisites.

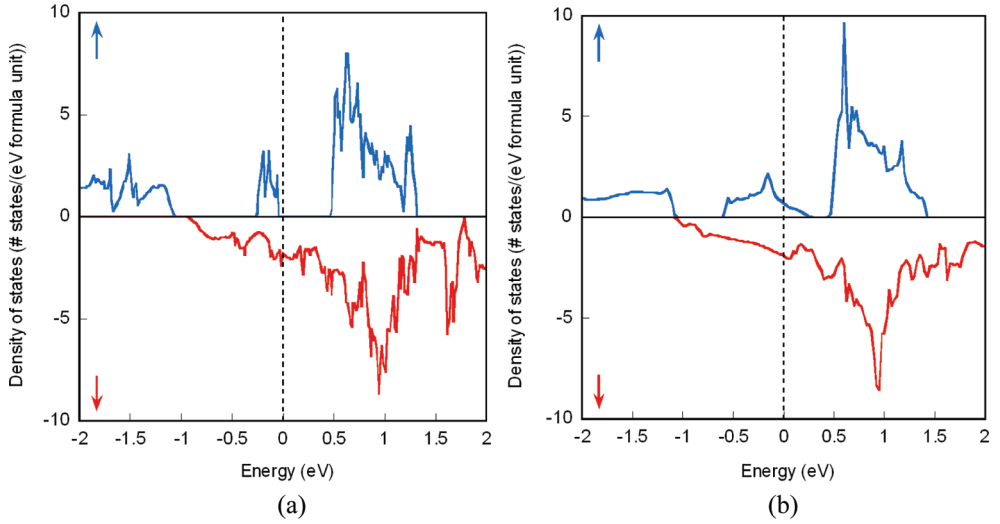

Figure 7. Total DOS for (a) $Sr_2Fe_{0.875}Mo_{1.125}O_6$ and (b) $Sr_2Fe_{0.75}Mo_{1.25}O_6$.

a kink at $x = 0$ for vacancy-dominated nonstoichiometry, in clear contrast to the experimental findings.

The shape of the theoretical M_s vs x curve in Figure 5b also is in good agreement with the experiment.[6] The agreement between the 40- and 80-atom results also demonstrates that a 40-atom supercell should be of sufficient size. The observation that the experimental moment is smaller than predicted, by a fairly constant amount, is likely a result of Fe/Mo antisite disorder in the experimental samples, as shown in the next section. However, a more careful analysis of the slopes of the M_s vs x curve, in both Mo-rich and Fe-rich parts, results in significant differences to the model predicted by Topwal et al.,[6] where the valence of the Mo atoms was assumed to change from +4 for $x = -1$ (i.e., in $SrMoO_3$) to +6 for $x = 0.33$, while leaving the valence of Fe atoms fixed at +3. Working with this assumption and taking out the contribution of antisite disorder from their results would give us a slope of 5.2 μ_B/x for $x \leq 0$ (Mo-rich), and -2 μ_B/x, for $x \geq 0$ (Fe-rich). In contrast, we find the slope to be 3.9 μ_B/x for $x \leq 0$ (Mo-rich), and -2.8 μ_B/x for $x \geq 0$ (Fe-rich).

To understand the reason behind the difference in slopes in the Mo-rich region, we consider a simplified picture. To begin with, at $x = 0$, we assume that the Fe atoms have five spin-up valence electrons while the Mo atoms have one spin-down valence electron. Taking a Fe atom out, would thus remove five spin-up electrons from the system. The single electron from a Mo atom that replaces the Fe atom could either be depolarized (i.e., have an equal probability of being present in the majority or the minority spin channel) or it could be spin-polarized and occupy the majority channel. The former scenario would lead to a slope of 5 μ_B/x (as suggested by Topwal et al.[6]), whereas the latter would lead to a slope of 4 μ_B/x (present calculations). The difference from the exact values of the slopes could be attributed to the change in valence of Fe and Mo ions with nonstoichiometry. We find the Mo_{Fe} sites to be strongly spin-polarized. Table 3 gives the average moment of Mo atoms at Mo sites (Mo_{Mo}), Mo atoms at Fe sites (Mo_{Fe}), Fe atoms at Fe sites (Fe_{Fe}), and Fe atoms at Mo sites (Fe_{Mo}) for the different values of x. Toward the Mo-rich ($0 \geq x \geq -1$) limit, the moment on the Mo_{Fe} atoms decreases systematically from a high value of 0.90 μ_B/atom at $x = -0.125$ to a low value of 0.23 μ_B/atom at $x = -0.875$. We also find that the absolute value of the moment on Mo_{Mo} atoms decreases as the excess Mo increases. This would eventually lead to a totally depolarized compound at $x = -1$ ($SrMoO_3$) and can be associated with the reduction of T_C that was observed by Topwal et al.[6] Similarly, a higher slope of -2.8 μ_B/x in the Fe-rich region ($x \geq 0$) suggests that the depletion of conduction electrons from replacing Mo atoms with Fe atoms occurs at a slower rate than assumed in the previous model.

Table 3. Average Magnetic Moment on Mo Atoms at Mo Sites (Mo_{Mo}), Mo Atoms at Fe Sites (Mo_{Fe}), Fe Atoms at Fe Sites (Fe_{Fe}), and Fe Atoms at Mo Sites (Fe_{Mo}) for $Sr_2Fe_{1+x}Mo_{1-x}O_6$ Compositions with Different Values of x

	Average Magnetic Moment (μ_B/atom)			
x	Mo_{Mo}	Mo_{Fe}	Fe_{Fe}	Fe_{Mo}
0.25	−0.07		3.98	−3.87
0.125	−0.24		3.94	−3.89
0	−0.38		3.91	
−0.125	−0.24	0.90	3.88	
−0.25	−0.21	0.80	3.90	
−0.375	−0.20	0.56	3.91	
−0.5	−0.19	0.28	3.89	
−0.625	−0.16	0.28	3.89	
−0.75	−0.06	0.24	3.90	
−0.875	−0.04	0.23	3.89	

Table 4 gives the average Bader charge on the Mo_{Mo}, Mo_{Fe}, Fe_{Fe}, and Fe_{Mo} atoms for nonstoichiometry in a 4 f.u. supercell. We find that, upon varying x from 0.25 to -0.75, the Bader atomic charges on Mo_{Mo} changes from $-1.60e$ to $-1.49e$ and for Fe_{Fe}, the change is from $-1.39e$ to $-1.29e$, respectively. Although it is difficult to estimate the exact valence changes from the Bader charges, they have been shown to reliably model trends for change in oxidation states.[30] In our case, the similar amount of change in the Bader charges on Mo_{Mo} and Fe_{Fe} atoms

(30) Jansen, M.; Wedig, U. *Angew. Chem., Int. Ed.* **2008**, *47*, 10026.

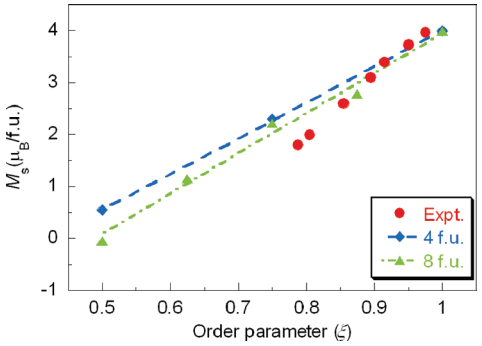

Figure 8. Variation of M_s with ξ. The experimental values are from ref 8.

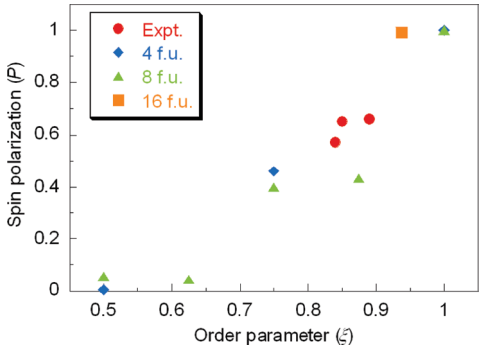

Figure 9. Spin polarization as a function of disorder in stoichiometric $SrFeMoO_6$. The experimental values are taken from ref 9.

Table 4. Bader Charge Analysis of Mo Atoms at Mo Sites (Mo_{Mo}), Mo Atoms at Fe Sites (Mo_{Fe}), Fe Atoms at Fe Sites (Fe_{Fe}), and Fe Atoms at Mo sites (Fe_{Mo}) for $Sr_2Fe_{1+x}Mo_{1-x}O_6$ Compositions with Different Values of x

	Bader Atomic Charge (e)			
x	Mo_{Mo}	Mo_{Fe}	Fe_{Fe}	Fe_{Mo}
0.25	−1.60		−1.39	−1.38
0	−1.57		−1.36	
−0.25	−1.55	−1.55	−1.35	
−0.5	−1.53	−1.53	−1.32	
−0.75	−1.49	−1.50	−1.29	

indicates that both of them change their valence relative to x. Our calculations thus give support to the experimental results by Rager et al.,[31] where a change of the valence of Fe atoms with increasing x from +2 to +3 has been suggested, in contrast to the fixed valence of Fe proposed by Topwal et al.[6]

The change in the oxidation states of the Fe and Mo ions also changes their ionic sizes, which, in turn, reflects the observed changes in lattice parameter with x (see Figure 5a). For example, for $x = -0.75$, the average Bader volume of Mo_{Mo}, Mo_{Fe}, and Fe_{Fe} ions is found to be 7.85, 8.50, and 7.63 Å^3, respectively. The sum of the volumes of all the Mo and Fe ions is 64.54 Å^3. For $x = 0.25$, the average volume of the Mo_{Mo}, Fe_{Fe}, and Fe_{Mo} ions is 6.52, 7.26, and 7.44 Å^3, respectively, with a sum over all the Fe and Mo ions of 56.02 Å^3. Thus on going from Mo-rich ($x = -0.75$) to Fe-rich ($x = +0.25$) not only does the antisite volume decrease (from 8.50 Å^3 to 7.26 Å^3), the Fe_{Fe} and Mo_{Mo} volumes also decrease by 4.8% and 17%, respectively. The decrease in volume of all three sites explains the observed decrease in lattice parameter with increasing x.

3.5. Disorder. As discussed previously, even in stoichiometric Sr_2FeMoO_6 samples, disorder involving Fe occupying the Mo sublattice and vice versa (Fe/Mo antisite disorder) almost always is present. Figure 8 shows the calculated change in the M_s value with the disorder parameter ξ for 40- and 80-atom supercells, along with the experimental values reported in ref 8. We find that the M_s value decreases strongly with decreasing ξ, because of the ferrimagnetic coupling between the Fe_{Fe} and Fe_{Mo} atoms. The orientation of the magnetic moments on the Mo_{Fe} atoms is strongly dependent on their nearest neighbors, as mentioned earlier in section 3.3. Nevertheless, this has a very small influence on the M_s value of the supercell, since the Mo atoms carry only a small moment. We also observe that, with disorder, Sr_2FeMoO_6 undergoes a half-metal-to-metal transition, because of the t_{2g} band of both Mo_{Fe} and Fe_{Mo} antisites at the Fermi level. This leads to a rapid decrease in spin polarization with increasing disorder, as shown in Figure 9, where we plot the spin polarization of the lowest energy configuration for every value of ξ. To probe the exact nature of the change of spin polarization with very small amounts of disorder, we performed an additional calculation with a 160-atom (16 f.u.) body-centered cubic (bcc) primitive cell with $\xi = 93.75\%$. We find that the spin polarization remains ~100% only for very small amounts of disorder. For $\xi = 93.75\%$, the spin polarization is ~98.9%, below which it decreases rapidly to a value of ~39%−44% for ξ values within a range of 75%−87.5%. Below $\xi = 75\%$, Sr_2FeMoO_6 loses its spin polarization completely. However, to identify the exact trend of change of spin polarization with disorder, still larger supercells would be required with excessive computational costs. Our values of spin polarization compare well with the recently published experimental results by Panguluri et al.[9] They are also in qualitative agreement with the model Hamiltonian calculations by Aguilar et al.[32]

Figure 10 shows the spin-resolved DOS for $\xi = 93.75\%$ (Figure 10a) and $\xi = 87.5\%$ (Figure 10b). For small amounts of disorder, the Mo_{Fe} and Fe_{Mo} t_{2g} states in the majority spin channel are strongly localized, with one of the peaks lying exactly on the Fermi level. Increased disorder leads to increased interaction between the defects, which causes these localized states to evolve into bands, as shown in Figure 10b. This indicates that even small amounts of disorder can start to deteriorate the half-metallicity, making it highly undesirable for spintronics applications.

3.6. Oxygen Vacancies (V_O). Small concentrations of V_O (up to 7%) have been found in experimental samples grown especially at low oxygen partial pressure ($p(O_2)$), which is typical for thin film growth.[7] Töpfer et al. reported a general decrease in the M_s value down to a

(31) Rager, J.; Zipperle, M.; Sharma, A.; MacManus-Driscoll, J. L. *J. Am. Ceram. Soc.* **2004**, *87*, 1330.

(32) Aguilar, B.; Navarro, O.; Avignon, M. *Europhys. Lett.* **2009**, *88*, 67003.

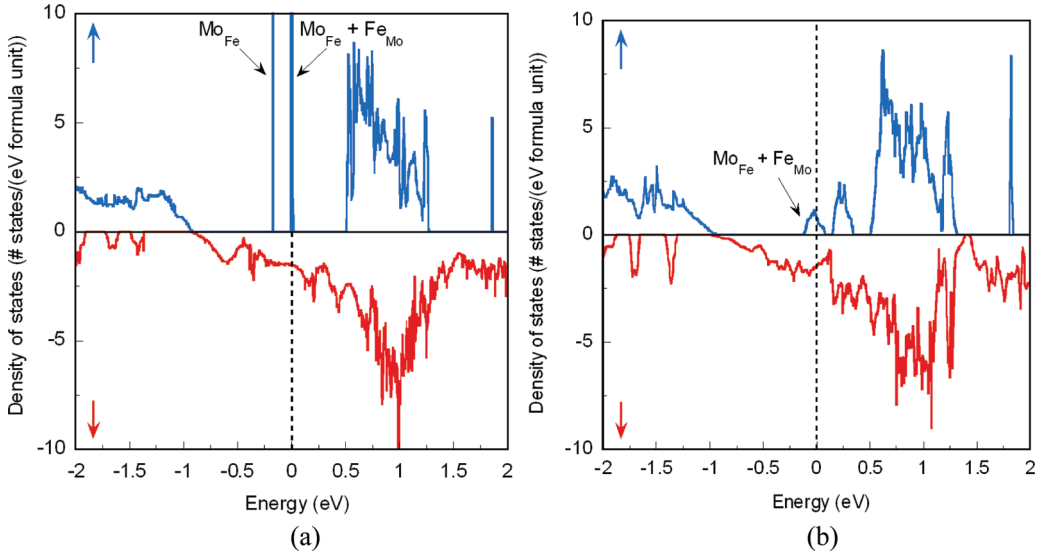

Figure 10. (a) Total density of states (DOS) for Sr_2FeMoO_6 with (a) $\xi = 0.9375$ and (b) $\xi = 0.875$. t_{2g} states from the Mo_{Fe} and Fe_{Mo} atoms have been marked.

final value of 3.3 μ_B at $C(V_O) = 6\%$.[7] Showing a similar trend, our results find that the M_s value decreases to 3.54 μ_B for a single V_O in a 40-atom supercell ($C(V_O) = 4.2\%$) and to an only marginally smaller value of 3.51 μ_B for two V_O ($C(V_O) = 8.4\%$). For both cases, half-metallicity is retained and, hence, 100% spin polarization is predicted.

3.7. Strong Localization Effects for O and Mo Orbitals. There have been a few reports where strong localization in the O 2p orbitals was suggested to be crucial to explain the properties of some transition-metal oxides.[33] Ray et al.[34] have shown that, in their Hartree−Fock model of Sr_2FeMoO_6, adding $U_{eff} = 2.85$ eV for the O 2p orbital electrons improved the match of the electron DOS with photoemission spectra, thus suggesting the presence of strong electron localization in the O 2p orbitals, as a result of hybridization with the transition-metal elements. However, we did not find any significant shift in the DOS when adding $U_{eff} = 2.85$ eV for the O atoms. We also did not find it necessary to add U to explain the magnetic and structural properties. Specifically, adding U for the O atoms resulted in only a small increase of 0.05% in the M_s values, accompanied by a 0.1% decrease in the lattice parameter values for all of the above cases, compared to the results obtained without U for O. These results suggest that there is no strong localization in the O 2p orbitals that affect the magnetic and structural properties in Sr_2FeMoO_6 in a meaningful way. Similarly, from the orbital-resolved DOS of perfect Sr_2FeMoO_6 (see Figure 2b), we can see that there is a significant overlap between the Fe t_{2g}, Mo t_{2g}, and the O 2p states in the minority channel below ε_F, implying sharing of electrons between the three species. Also, a magnetic moment of −0.4 μ_B on each Mo atom in perfect Sr_2FeMoO_6 is consistent with delocalization of the minority spin electron. Hence, to probe if the Mo 4d electrons are itinerant or localized, we add an U_{eff} value of 1 eV for Mo atoms and observe negligible effects on M_s (changes of ~0.01 μ_B/f.u.) and band structure, thus indicating that the Mo 4d electrons are indeed itinerant.

4. Conclusions

We have successfully described the structural, electronic, and magnetic properties of ordered and stoichiometric Sr_2FeMoO_6 by performing spin-polarized GGA+U calculations. Our calculations show that nonstoichiometry in Sr_2FeMoO_6 should be almost exclusively regulated by metal-ion antisites, with vacancies having a formation energy significantly higher by several electron volts. Our predictions of the change in lattice parameter and M_s, in response to $Sr_2Fe_{1+x}Mo_{1-x}O_6$ nonstoichiometry, are in excellent agreement with experiments. The decrease in lattice parameter with increasing x is a result of the change in oxidation states of the Mo and Fe atoms and the associated change in their Bader volumes. The results also suggest that not only does M_s decrease in Mo-rich samples as the Mo_{Fe} antisite concentration increases, but that the half metallicity is lost for Mo enrichment in excess of ~12.5%, because of the t_{2g} states of Mo_{Fe} antisites, which cross the Fermi level. Along with that, the spin polarization decreases as the Mo enrichment increases to more than 12.5%, until the spin polarization disappears at an enrichment of ~75%. If the stoichiometry changes in the opposite direction, toward Fe-rich samples, the Fe_{Mo} antisites couple ferrimagnetically with the Fe sublattice, reducing M_s but retaining half-metallicity and 100% spin polarization.

The presence of oxygen vacancies causes a small decrease in M_s and leaves the half-metallicity intact. Finally, Fe/Mo antisite disorder in stoichiometric samples leads to a strong, almost-linear decrease in M_s as the disorder increases and destroys the half-metallicity, because of the presence of both Mo_{Fe} and Fe_{Mo} antisites and the related

(33) Korotin, M.; Fujiwara, T.; Anisimov, V. *Phys. Rev. B* **2000**, *62*, 5696.
(34) Ray, S.; Mahadevan, P.; Kumar, A.; Sarma, D. D.; Cimino, R.; Pedio, M.; Ferrari, L.; Pesci, A. *Phys. Rev. B* **2003**, *67*, 85109.

t_{2g} bands. The energy of the disordered cell is strongly dependent on the nearest neighbors around the antisite. We find that the formation energy of disorder is lower for neighboring antisites than separated antisites, suggesting that short-range ordering is favorable, as observed in recent experiments. The attraction between the antisites is largely driven to avoid formation of energetically less favorable Fe−O−Fe and Mo−O−Mo type bonds over more favorable Fe−O−Mo bonds. Local strain relaxation around the antisites plays an important role and is intimately linked to the redistribution of charges around them. Finally, the spin polarization remains close to 100% only for very small amounts of disorder ($\xi \geq 93\%$), whereas for higher amounts of disorder, it decreases rapidly.

Acknowledgment. The authors acknowledge funding for this project by the Center for Emergent Materials at the Ohio State University, an NSF MRSEC (Award No. DMR-0820414). We would also like to thank Prof. D. D. Sarma (Indian Institute of Science) for very fruitful discussions. Computer calculations were performed at the Ohio Supercomputer Center (under Grant No. PAS0072).